LA-UR -78-1973

MASTER

CONF-780811--24

TITLE: LASL TOROIDAL REVERSED-FIELD PINCH PROGRAM

AUTHOR(S): D.A. Baker, C.J. Buchenauer, L.C. Burkhardt, C.K. Chu,* J.N. Di Marco, J.N. Downing, A. Haberstich, R.B. Howell, A.R. Jacobson, H.J. Karr, P.C. Liewer,**, E.M. Little, M.D. Machalek, W. Park,* A.E. Schofield, A.G. Sgro, K.S. Thomas, and P.C. T. Van der Laan***

SUBMITTED TO: IAEA Conference, Innsbruck, Austria
August 23-30, 1978

*Columbia University, New York City, NY USA
**University of Maryland, College Park, Md. USA
***Present address: EEg Group EHO, Eindhoven Univ. of Technology, P.O. Box 513, Eindhoven, The Netherlands

UNITED STATES
ENERGY RESEARCH AND
DEVELOPMENT ADMINISTRATION
CONTRACT W-7405-ENG-36

BLANK PAGE

LASL TOROIDAL REVERSED-FIELD PINCH PROGRAM*

D.A. Baker, C.J. Buchenauer, L.C. Burkhardt, C.K. Chu,** J.R. DiMarco, J.N. Downing, A. Haberstich, R.B. Howell, A.R. Jacobson, H.J. Karr, P.C. Liewer,† T.M. Little, M.D. Machalek, W. Park** A.E. Schofield, A.G. Sgro, K.S. Thomas, and P.C.T. Van der Laan‡‡
Los Alamos Scientific Laboratory, Los Alamos, New Mexico U.S.A.

ABSTRACT

The determination of the absolute energy loss due to radiation from impurities in the LASL toroidal reversed-field pinch experiment ZT-S is reported. The measurements show over half of the energy loss is accounted for by this mechanism. Thomson scattering electron density measurements indicate only a gradual increase in temperature as the filling pressure is reduced indicating an increased energy loss at lower pressures. Cylindrical and toroidal simulations of the experiment indicate either that a highly radiative pinch boundary or anomalous transport are needed to match the experimental results. New effects on the equilibrium due to plasma flows induced by the toroidal geometry are predicted by the toroidal simulation. The preliminary results on the low temperature discharge cleaning of the ZT-S torus are reported. A description of the upgrade of the ZT-S experiment and the objectives, construction and theoretical predictions for the new ZT-40 experiment are given.

---

*Work performed under the auspices of th U.S. Department of Energy.
**Columbia University, New York, New York USA.
†University of Maryland, College Park, Md.
‡‡Present address: EB; Group EH0, Eindhoven Univ. of Technology, P.O. Box 513, Eindhoven, THE NETHERLANDS

I. INTRODUCTION

The toroidal reversed-field ...ach approach continues to be motivated by its promise of high-beta, stable equilibrium configuration with the possibility of ohmic heating to ignition with moderate magnetic fields. Further advantages stem from the freedom of choice of aspect ratio that gives an escape from possible adverse trapped-particle effects and can lead to a simpler modular construction with easier access as compared to a compact torus.

The Los Alamos program is currently centered around the 15-cm bore ZT-S experiment (a modification of the earlier 10 cm bore ZT-I experiment) and the 40-cm bore ZT-40 experiment presently under construction. Studies between the ZT-I and ZT-S experiments showed the confinement time scaling proportional to the square of the minor diameter are reported in Ref. [1]. More recent efforts on the ZT-S experiment have been concentrated on the measurement of the radiation loss from impurities and in the study of the raising of the electron temperature by operating at lower filling pressure and by the use of low temperature discharge cleaning.

The ZT-40 experiment is expected to begin preliminary physics in calendar year 1979. The experiment has been designed to allow versatility in its range of risetimes (2.5 μs-1 ms). It will allow the study of programmed reversed-field profiles as well as configurations obtained by self reversal. The general aim of ZT-40 is to obtain physics information needed to predict the optimum design of subsequent larger devices.

II. ZT-S

A. General

A chief factor limiting the confinement time in the ZT-S reversed-field experiment after favorable plasma-field profiles are produced is the deterioration of the stability of the configuration with time due to resistive effects [1]. The measured electron temperatures are low and field diffusion rates are high. The general objectives have been to (1) determine the nature and magnitude of the radiation loss, (2) operate at lower filling pressure in an attempt to raise electron temperature, (3) design and test a discharge cleaning scheme, (4) design, build, and test a power crowbar circuit to lengthen useful time of the field. The experiment was then upgraded to improve the following: vacuum cleanliness, versatility in the changing of the field programming, and diagnostics.

B. Radiation Loss Measurements

1. Nature and level of impurities. Spectroscopic and mass analyzer measurements of the ZT-S discharge have shown that the main impurity is oxygen with smaller amounts of carbon and nitrogen. The impurity number density is in the range from ~ 0.3% to ~ 1% of the deuterium fill. Theoretical calculations [2] predict serious energy losses that can cause limitations on the electron temperatures for the current and plasma densities being studied.

2. Absolute Measurements of the Radiation Loss

(a) Method. A survey of the impurity lines was made spectroscopically to determine the spectral range of the line radiation emitted from the ZT-S plasma. The wavelength region containing the substantial portion of radiation is between 200-1600 Å. A fast system that was sensitive to vacuum ultraviolet radiation was arranged to view the ZT-S pinch through a pump port. A schematic of the detector arrangement is shown in Fig. 1. Basically the detecting system consists of a fast, linear photodiode of wide dynamic range. The detector is sensitive to visible wavelengths and is used with a sodium salicylate phosphor wavelength shifter that intercepts the photons emerging from the plasma. The

fluorescence emission spectrum of the phosphor varies by a factor of 1.45 from 2500 Å to 1200 Å and then is flat down to 200 Å. The fluorescence spectrum centers at ~ 4200 Å well within the high sensitivity range of the photodiode.

The radiation from the plasma in the ZT-S discharge passes through the aperture in the alumina plug inserted into the pump port and then through two successive 1-cm-diam apertures to the detector. The last two apertures are covered with a wire mesh grid to improve the detector shielding against electrical noise. The signal from the detector is amplified and then transmitted to an oscilloscope display.

(b) Results. The analysis and interpretation of the results of the measurements involve several factors: (1) the calibration of the detector, (2) the source and detailed solid angle corrections, (3) the determination of mean photon energy. Since the measurement was made through a single port, assumptions about the source distribution are needed to make determinations of the absolute value of the total radiative energy loss. Toroidal symmetry is assumed and comparisons with a variety of reasonable radial source distributions show these to alter the deduced loss over a range of about a factor of two.

For an assumed source distribution having a sharp boundary plasma with a flat emission profile, the measurements give a radiative loss of 5 to 8 MJ per meter length during the ~ 30 μs stable time of the discharge. The total energy balance for a sample discharge is shown in Fig. 2. The two curves show the energy input and energy content per meter of length (plasma + field energy) of the discharge as a function of time as deduced from current, voltage, and magnetic probe data. For comparison, the difference between the two curves, which represents the energy loss, is shown in Fig. 3 along with the radiation loss as deduced from the above detector measurements. The same radiation loss curve is compared with the calculated ohmic heating for T_e = 15 eV in Fig. 4. The curves indicate that essentially all of the loss is due to the radiation. In view of the factor of ~ 2 uncertainty in the absolute radiation measurement mentioned earlier, this agreement is fortuitous. The measurement does indicate however that the radiation contributes half or more of the energy loss.

For plasma temperatures of 15-20 eV, as measured for ZT-S from Thomson scattering (see next section) and spectral impurity ionization state measurements, a calculation of the theoretical radiation loss rate gives values of 8-10 MW per meter. The radiation loss rates were computed for assumed values of T_e using Ortolani's PRAD code [2] based on McWhirter's radiation loss equation [3] with a multiplying factor of 5 as suggested by the Maryland Group results. [4] This agreement is better than expected in view of the uncertainties in the measurements and the approximations made in the functions used in determining the ionization, excitation, and emission processes.

(c) Conclusions. The conclusions of these studies are as follows: for ZT-S operating at I ~ 60 kA and a filling pressure of 20 mtorr, (1) the radiation loss is ≥ 50% of the energy loss, (2) the radiation is primarily in the vacuum uv with a mean energy of ~ 30 eV (λ ~ 400 Å), (3) the chief impurities are oxygen and carbon, (4) these losses are comparable to those predicted by theory.

C. Electron Temperature Measurement

1. General. Thomson scattering measurements of electron temperature at filling pressures of 18 and 34 mtorr in ZT-S have been reported earlier. [1] Operation was studied at lower fill pressures to see if higher electron temperatures and lower diffusion rates can be obtained. Earlier measurements at lower densities were then hampered by instrumental scatter-

tor. This problem has been resolved by the addition of two 69-3 Å notch filters to the scattered spectrum detector. The width at half maximum of each filter is 16.2 Å. The overall sensitivity of the detector is reduced by a factor of 2, whereas the instrumental scattering signal is down by a factor of 15. Good data have been obtained at filling pressures of 10 mtorr. Data acquisition at 5 mtorr is limited by the reproducibility of the pinch rather than by the sensitivity of the diagnostic. The field diffusion at ≤ 5 mtorr gas fill and lower was observed to be very rapid.

2. Results. The temperature measurement shown in Fig. 5 have been obtained with a filling pressure of D_2 of 10 mtorr, and a peak toroidal current of 60 kA with an initial rise of 35 kA/μs. The initial bias field was set at 0.065 T and the toroidal field at the wall reversed to -0.079 T in about 8.5 μs. The postimplosion plasma radius as estimated from pressure profiles was of the order of 4 cm.

The square data points have been obtained with a polychromator dispersion of 33 Å/mm and the circles with a dispersion of 66 Å/mm. The solid circles are the result of a least squares fit to 7 polychromator channels. The open circles are based on the same data, but using the two closest channels only on each side of the 6943 Å channel. The difference between the two analyses is relatively minor at late time in the discharges (> 15 μs). At early times, however, the analysis based on 4 data points gives a much lower temperature and, perhaps, a better representation of the main body of the electron distribution than the 7-point analysis.

Figure 5(a) shows a peak central value of T_e of 25 eV which then decays gradually to 15 eV at 25 μs. The electron temperature at 1.5- and 3-cm radii levels off at about 15 eV. There is an indication of a higher temperature sheath at $r \geq 4.5$ cm at early times.

3. Conclusions. Comparison of this result with the previous T_e measurements indicates only a small increase of the electron temperature as the fill pressure decreases. The peak values of T_e reported earlier [1] were 12 eV at 24 mtorr and 15 eV at 18 mtorr. The operation at lower fill pressures does not show temperatures scaling inversely with the fill density as simple models would predict. A possible explanation is that there is either reduced thermal transport or more wall impurities released at the lower fill pressure operation.

V. Discharge Cleaning Studies

1. Motivation. The foregoing radiation loss and T_e studies indicate the need for determining if suitable discharge cleaning methods can be developed in order to reduce the impurity level to acceptable limits. A preliminary investigation was made to determine the usefulness of the low temperature discharge technique [5] for the removal of the loosely bound surface impurities from an alumina discharge vessel. Previous work in this area has been limited to metal-walled systems. It is known, however, from the results of the Petula group at Grenoble that the replacement of a tungsten limiter with an alumina one can reduce the oxygen in the discharge a factor of three to four in the Petula tokamak [6].

2. Discharge Cleaning Circuit. The discharge cleaning circuit consists of capacitor and switching circuit capable of delivering ~ 110 J per pulse to a series connection of the toroidal and poloidal field circuits. This arrangement forms a 2 kA screw pinch and is capable of producing one to five pulses per second. The circuit can be quickly removed from the experiment by the use of a pair of pneumatically operated switches thus minimizing the time between the cleanup discharges and the normal firing of ZT-S.

The energy input per pulse varied from 50 J at 0.7 mtorr to 160 J at 40 mtorr gas fill.

The confirmation of the required low electron temperature of the plasma during discharge cleaning was obtained by two methods. First the resistivity of the plasma was calculated from the voltage and current traces. Using the Spitzer equation and obtaining the plasma radius from the streak pictures we find 2-3 eV for the filling pressures of 1, 10, and 20 mtorr. The second method was a line-to-continuum measurement using Dβ 4861 . From this we found 3.0 eV at 10 mtorr and 2.0 eV at 1 mtorr.

3. Results. The mass analyzer has been used to observe the gases that are pumped from the torus before and during discharge cleaning. The principal mass numbers observed are 14, 16, 18, 19, 20, and 28. These correspond to N, O or CH_4, H_2O, HDO, D_2O, and CO or N_2. The ambiguity between D_2O and CD_4 was resolved by comparing results between hydrogen and deuterium discharges.

The mass analyzer was used to monitor the D_2O line during the discharge cleaning. With the turn on of discharge cleaning there is an increase in D_2O. The amplitude of this signal decreases rapidly in the first few minutes and then levels off. When the discharge cleaning is terminated, the D_2O decreases immediately. When the gas flow is terminated the D_2O further decreases usually below the initial level present.

4. Conclusions.

(1) Oxygen impurity was converted to water generated by the 2-5 eV plasma and is pumped from the system as has been observed with metal systems [5]. This was done without overheating the polyethylene electrical insulation of ZT-S.

(2) Five hours of discharge cleaning reduced the effective outgassing rate a factor of two or more. Further reductions in total outgassing rate were limited by the torus construction (see Sec. E below).

(3) In addition to water, the next most abundant impurity observed on the mass spectrograph was found to be mass 28 (CO or N_2).

(4) A simple capacitive discharge circuit allowing immediate switching between discharge cleaning and normal high voltage operation has been demonstrated to be practical for this application.

E. ZT-S Upgrade

1. Description of Upgrade

Since impurity radiation losses may be dominating the physics of the plasma behavior, it was decided to upgrade the cleanliness of the vacuum system. The alumina torus was made from ninety segments joined using viton O-rings. Although these O-rings were well protected from the plasma, they do constitute a significant outgassing load which cannot be corrected by discharge cleaning. Ideally one would solve this problem by using a solid torus. Although the procurement of such a torus with adequate diagnostic windows may be a future prospect, it is not possible on a short time basis. Instead the number of O-rings can significantly be reduced by a special glass joining technique [7]. The elements of the present ZT-S upgrade were as follows:

(a) Improved Vacuum System. (1) Reduction of number of O-rings in the system from 90 to 24. (2) No vacuum grease permitted. (3) The use of a new air bearing totally oil-free turbomolecular pump. (4) Improved effective pumping speed a factor of three. (5) Use of a quick change-over low temperature discharge cleaning system.

(b) Improved Circuitry. (1) Power crowbar system (2) New toroidal field circuit allowing more flexibility in setting up the RFP configuration.

(c) Improved Diagnostics. (1) New small, high resolution magnetic probes. (2) New improved data acquisition system. (3) Newly developed five channel interferometer [8]. This will allow the measurement of the integrated electron density along five parallel chords simultaneously. A schematic of the arrangement is shown in Fig. 6.

At the time of this writing the upgraded machine has just become operational.

IV. ZT-40

A. Objectives

The ZT-40 experiment is the next step beyond the ZT-S in the Reverse Field Pinch program at LASL. The initial objective of ZT-40 will be to demonstrate confinement time scaling from the results of ZT-1 and ZT-S. If the confinement time scales as the square of the minor bore, ZT-40 will be stable for at least 150 to 200 μs. A second objective will be to operate in a regime clean enough to overcome the impurity radiation barrier and raise the temperature to at least $T_i = T_e \sim 100$ to 200 eV. The actual temperatures achievable will depend upon the useful upper limit on current density, the lower limit of the operating plasma density and the losses. If the diffusion coefficient becomes lower due to the higher T_e values longer confinement times can be expected. The power-crowbarred fields of ZT-40 can be sustained for ~ 3.5 ms. An upper limit on T_i and T_e to be expected assuming classical ohmic heating and good confinement for 3 ms for various ion densities can be seen from the curves in Fig. 7 obtained from the Ingrad code [2]. Shown also is the effect of 0.5% oxygen impurity. No thermal transport losses are included. To maximize the ion temperature, an operating density of 5×10^{13}–1×10^{14} cm^{-3} is indicated. In addition, ZT-40 will be used to determine the ranges of the current and electron densities which allow the production of stable configurations. Of particular interest is to determine whether there are any microinstabilities which impose an upper limit on the usable ohmic heating current. Another objective is to operate with reduced rates of rise of current in order to establish the time scale over which the stability can be controlled by programming of external currents. The self reversal method of production of reversed field configurations will be studied as a function of risetime. An overall objective of the studies is to determine the optimum operation between the generally competing reactor requirements of slow risetime and low start up energy losses.

B. Description

ZT-40 has a 40-cm minor bore torus with plasma aspect ratio of 5.7. The torus can be fed at a maximum of 12 points and has 12 magnetic cores equally spaced about the torus. A drawing of the ZT-40 experiment is shown in Fig. 8. The maximum number of feedplates allowed in the design was determined by the requirement that the minimum allowable initial risetime of the current be the same as ZT-S (2.5 μs). The current risetime is lengthened to ~ 20 μs by removing feedplates and shorting the respective toroidal feed points, and by series-paralleling the poloidal field windings. Very slow operation (40 μs to 1 ms) can be attained by removing all feedplates and inducing the toroidal current by means of toroidal windings on the outside of the primary or by energizing the field only with the power crowbar banks.

The initial experiments on ZT-40 will utilize a ceramic discharge tube. Further experiments with metal tubes are planned for the slower experiments if their use can be shown to lead to cleaner discharges. The discharge tube is located inside a 2-cm-thick aluminum stabilizing shell

which serves as the primary conductor of a transformer with the plasma as the secondary.

The vacuum system has been designed to be oil-free and allows rapid pulse discharge cleaning and in-situ baking of the vacuum chamber.

The basic machine parameters for ZT-40 are given in Table I.

TABLE-I

ZT-40 DESIGN PARAMETERS

Major Radius	$R = 114$ cm
Minor Vacuum Chamber Radius	$a = 20$ cm
Gas Fill (D_2)	$p = 5$-30 mtorr
Electron Density	$n_e = 10^{14}$-10^{16} cm^{-3}
Toroidal Current	$I_\phi \sim 150$-600 kA
Mean Toroidal Current Density	$J_\phi \leq 2$ kA/cm^2
Initial (toroidal) Field	$B_\phi = 0.2 - 0.6$ T
Reversed-toroidal Field	$B_{\phi_R} = \leq -0.5$ T
Poloidal Field	$B_\theta = \leq 0.6$ T
Range of Plasma Current Risetime	$\tau = 2.5$ μs to 1 ms
Base Pressure	$p_0 \sim 10^{-7}$ torr

V. THEORY

A. One Dimensional Hybrid Simulations

The LASL one-dimensional hybrid code [9,10] has been used to study the evolution of the magnetic field and temperature profiles of the ZT-S experiment. Anomalous bulk transport coefficients were required to achieve agreement with the measured profiles. The anomalous electrical resistivity used in previous calculations of ZT-I [9] were found to adequately describe the implosion and early post implosion field diffusion in ZT-S (i.e., up to 3 μs), as illustrated in Fig. 9(a). Also as found for ZT-I [9] classical resistivity alone did not account for the observed diffusion because the heating in the low density outer portion of the sheath caused the resistivity to drop, inhibiting further diffusion. Including oxygen impurity radiation with the assumption that the oxygen density is either proportional to the compressed deuterium density or constant (the latter intended to mock up wall emission of oxygen) lowers T_e in the dense core of the plasma but does not eliminate the high temperature (~ 100 eV) in the sheath. It presumably would be possible to devise, with much trial and error computing, a wall emission rate that would load the region with oxygen in such a way as to reduce the high sheath temperature. Except for the latter possibility, the observed field diffusion must be a result of an anomalous resistivity.

A large anomalous resistivity is required to fit the field data during the implosion. However, at later times the resistivity must decrease. A calculation using the Chordura formula with the same coefficients throughout the calculation showed that the axial field profile collapsed to about 30 to 50% of the observed field at 10 μs and remained much lower than the observed field thereafter. In addition it is found that $T_e \geq 100$ eV everywhere in the plasma at 15 μs, whereas the observed T_e is less than 30 eV. Theoretically this drop in anomalous resistivity is expected, since the high velocities and steep gradients which may drive the turbulence during the implosion decrease afterward. In fact, measurements by Commisso and Griem [11] demonstrated a factor of 5 to 10 decrease in the turbulent fluctuation energy and resistivity after the implosion on the University of

Maryland θ-pinch. Field profiles at 12.3 μs from a ZT-S calculation with Chodura coefficients decreased by a factor of five after the first peak compression are compared with experiment in Fig. 9(b). Note that now the height of the axial field profile agrees with experiment (although the width of the profile is a bit too narrow) and the experimental and theoretical $\dot{B}_z$ profiles show a similar structure. In this calculation radiation from oxygen impurities having a constant density profile with a value 0.7% of fill density was included. In a previous calculation without the radiative loss the plasma temperature reached 100 eV everywhere at 15 μs (although the field profiles were similar to those in Fig. 9(b)). In Fig. 10 T_e at 1.5 cm is plotted as a function of time for the calculation which included losses. Note that these temperatures are quite consistent with the measurements in Fig. 5(b). During the 15 μs calculation for a power loss of about 10 MW per meter which is comparable to the average measured power loss reported in Sec. II(b).

In conclusion, the anomalous resistivity used to model the early time behavior of ZT-I also describes the early time field diffusion in ZT-S. The later time behavior of ZT-S, with its enhanced confinement time, can also be modeled provided that the resistivity is decreased at late time to account for the expected decrease in the turbulent fluctuation energy. When impurity radiation from oxygen is included in the calculation, and the oxygen density is chosen to be within its experimentally determined range, the calculated and measured T_e are comparable.

Simulations with this code have also been done for ZT-40 parameters. The predicted field distributions for a 20 μs current rise and a programmed reversed field are shown in Fig. 11. Chodura anomalous resistivity is used. The simulations show that sheath thickness is comparable to those found in the previous ZT experiments so that with the larger radius of ZT-40, the poloidal field is well excluded from the main body of the pinch for well over 20 μs. The calculations indicate initial mean temperatures on the order of 100 eV. Further programming and studies of the stability of the resulting equilibrium profiles are in progress.

B. Time-Dependent Toroidal MHD Simulations

1. General. Two-dimensional MHD simulations of the LASL reversed field pinches ZT-I, ZT-S, and ZT-40 have been made.

The model used is the single-fluid, time-dependent, axisymmetric magnetohydrodynamic equations with dissipation. Initial conditions assume a fully ionized low temperature plasma at rest, with appropriate bias toroidal field. The equations are driven by time-dependent boundary conditions: the toroidal field and the poloidal flux are prescribed as functions of time in agreement with the experimental conditions. The poloidal flux is indirectly extrapolated from the prescribed toroidal current.

The only adjustable transport and dissipation parameters were the following:

(1) Electrical conductivity--both scalar classical Spitzer conductivity and Chodura [12] anomalous values were studied.

(2) Thermal conductivity--a constant value about equal to the classical parallel heat conductivity for a 4 eV plasma accounts for anomalous effects as well as radiation, not otherwise accounted for explicitly. Remarkably, the same constant value (2×10^6 cgs units) was found to apply to both ZT-I and ZT-S (as well as the Italian RFP ETA BETA and the Dutch screw pinch SP-I) in the sense that the predicted mean temperatures agree reasonably with experimental values.

(3) Numerical viscosity was used in momentum equations to give stability, but is small in effect compared to other dissipations.

(4) Low density cut-off in vacuum region equal to 5% of initial filling density.

The equations are solved numerically in an Eulerian grid in toroidal-polar coordinates, and the standard ADI method is used. [13-15]

2. Results for ZT-I and ZT-S

(a) Field-penetration. The diffusion of the magnetic field is more directly controlled by the electrical conductivity than by the other transport coefficients, and it is instructive to examine different experiments at the same time. Figures 12 and 13 show B_ϕ and B_z as functions of position at different time instants for ZT-I and ZT-S respectively. The dashed lines in Fig. 12 are obtained for a purely classical resistivity with a low T_e due to the anomalous thermal conductivity used. One concludes that for the temperature and current density ranges of these experiments, both classical (with anomalously low T_e) and Chodura resistivity give reasonable agreement, although during the initial setting up phase, the Chodura resistivity gives somewhat better comparisons.

(b) Longer time behavior. The simulation runs are carried out to near-equilibrium. For this later phase the anomalous resistivity gave poor comparisons and the actual resistivity appears to be close to classical. For ZT-S the radial oscillations in the calculation damped in ~ 6 μs in agreement with observation.

(c) Toroidal effects. This simulation does not have the same detailed physics as in many 1-D simulations, but it does give all toroidal effects automatically. The following particularly interesting toroidal phenomena should be noted. Figure 14(a) shows the toroidal shift of the magnetic axis versus time, and Fig. 14(b) shows the widely different current profiles along a vertical diameter and along a horizontal diameter of the poloidal plane, as a consequence of the toroidal shift. The toroidal shift is ~ 1 cm, about twice the shift computed assuming static equilibrium. This larger shift is evidently due to the toroidal plasma flow that can be seen in Fig. 15. These differences are important in interpreting measured results from experiments. In Fig. 15(a) are shown the three components of velocity in toroidal coordinates as functions of time at the two points indicated in Fig. 15(b). Prominently visible is a shear flow in the toroidal direction, induced by the $\vec{J} \times \vec{B}$ force in the poloidal plane (the toroidal curvature causes $\vec{J}$ and $\vec{B}$ to be not exactly parallel in the poloidal plane). It would be interesting to observe this flow in actual experiments.

3. Predictions for ZT-40.

Figure 16 shows the predicted early time field profiles for ZT-40 using Chodura resistivity. The temperature at early times is about 70 eV. In this case, the present method of calculation can at best give the correct initial behavior and dynamics but the correct late time behavior must be obtained from quasi-equilibrium type of diffusion calculations.

VI. ACKNOWLEDGMENTS

The authors wish to thank the LASL engineering group under the direction of C. F. Hammer for supplying the engineering for ZT-S upgrade and the ZT-40 design and construction. Thanks are also extended to R. Gerwin, L. W. Mann, and L. Turner who have supplied support in theoretical and computational areas.

REFERENCES

1. [illegible], D.A. et al., "Plasma Physics and Controlled Fusion Research 1974 (Proc. 5th Int. Conf. [illegible] 1974) 1, IAEA, Vienna (1977) [illegible].
2. [illegible], S. and [illegible], S., "Study of the Impurity Radiation Losses in a Pinch Discharge," UPEF 75/06, University of Padova, Italy (December 1975).
3. [illegible], "Spectral Intensities," in PLASMA DIAGNOSTIC TECHNIQUES, Richard H. Huddlestone and Stanley L. Leonard, Eds. (Academic Press, 1965). Chap. V., 201-263.
4. [illegible], Atomic Data for CTR, July 1975.
5. [illegible] L. and TAYLOR, R.J., "Trapping and Removal of Oxygen in Tokamaks," Nuclear Fusion 17, 1143-1151 (1977).
6. [illegible], R. et al., Plasma Physics and Controlled Fusion Research 1974 (Proc. 6th Int. Conf. [illegible], 1976) IAEA, Vienna (1977) 259.
7. [illegible] III and STODDARD, S.D., J. Am. Ceram. Soc. 57 [2], [illegible] (197[illegible]).
8. [illegible], "A Novel Interferometer for the Measurement of Plasma Density," Los Alamos Scientific Laboratory report LA-[illegible]727-MS (197[illegible]).
9. [illegible], A.C. and [illegible], C.W., Phys. Fluids 19, 126 (1976).
10. [illegible], A.C., ibid. 21, [illegible] (197[illegible]).
11. [illegible], R.J. and [illegible], ibid. 20 44 (1977).
12. [illegible], R., Nuclear Fusion 13, 55 (1973).
13. [illegible], [illegible], C.F., Phys. Fluids 18, [illegible] (1975).
14. [illegible], W., [illegible], C.F., Nucl. Fusion 17, 1190 (1977).
15. [illegible], Ph.D Thesis to appear as a Columbia University Lab report No. 75.

FIGURE CAPTIONS

Fig. 1. [illegible] detectors.

Fig. 2. [illegible]

Fig. 3. [illegible]

Fig. 4. [illegible]

Fig. 5. [illegible] scattering measurement of electron temperature at [illegible]

Fig. 6. Schematic of the [illegible] interferometer.

Fig. 7. [illegible] electron temperature [illegible]

Fig. 8. Artist's sketch of the front end of ZT-40.

Fig. 9. A comparison of the ZT-S field's theoretical calculations with the Lehigh 1-D code. The x's are the experimental poloidal field data (to be compared with the B_θ of the cylindrical code) and the ●'s are the toroidal field data [illegible] (a) field [illegible] (b) [illegible] after [illegible]

Fig. 10. Electron temperature as calculated [illegible] 1.5 [illegible] in ZT-[illegible].

Fig. 11. 1-D Hewitt code predictions of the field profile for ZT-40 with reversed-field programming. (a) axial field, (b) azimuthal field. Conditions: current rise time 20 μs, initial deuterium ion density [illegible] × $10^{1?}$ cm^{-3}, initial bias field 3 kG, peak pinch current 600 kA.

Fig. 12. ZT-S toroidal and poloidal field profiles: (a) 2-D toroidal calculation results with classical resistivity (---), and with the anomalous resistivity (-); (b) experimental curves (straight lines are drawn between data points).

Fig. 13. Toroidal and poloidal field profiles on the vertical radius ($\theta = \pi/2$) of the poloidal plane are compared between the toroidal 2-D calculation (---) and experiment (---) at 2.6 and 4.6 μs for ZT-S.

Fig. 14. (a) Time trace of the toroidal shift of the magnetic axis. (ZT-S) (b) Calculated toroidal current density profiles at 6.5 μs. The solid line represents the values on the vertical diameter ($\theta = \pi/2$) of the poloidal plane, and the dashed line on the horizontal diameter. (ZT-S)

Fig. 15. Time traces of the radial (U_r), azimuthal (U_θ), and toroidal velocities (U_ϕ at the point depicted in (b)). (ZT-S)

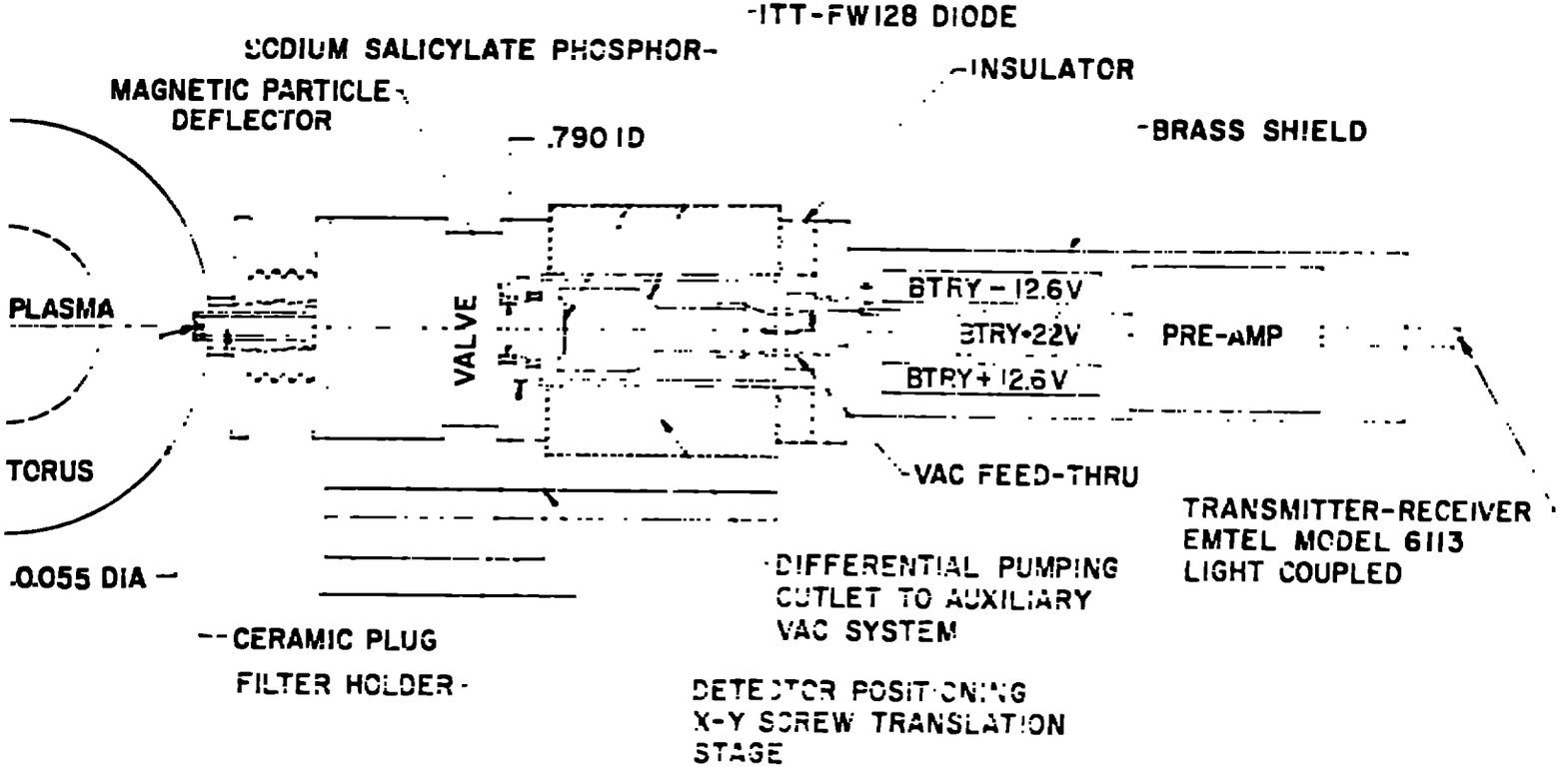

PHOTODIODE RADIATION ENERGY DETECTOR

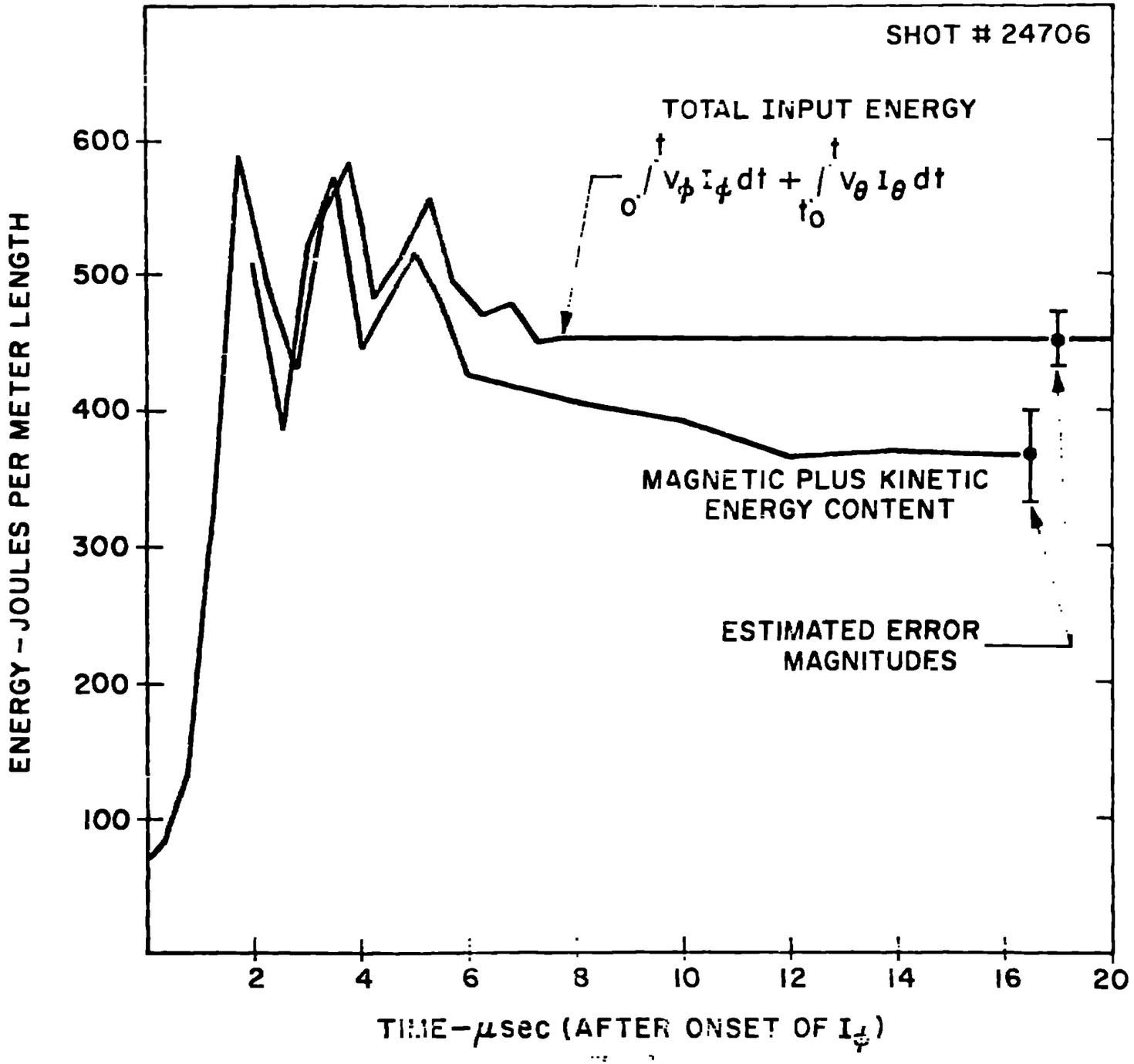

Fig. 2.

Current, magnetic plus kinetic energy, and total input energy in Shot 24706.

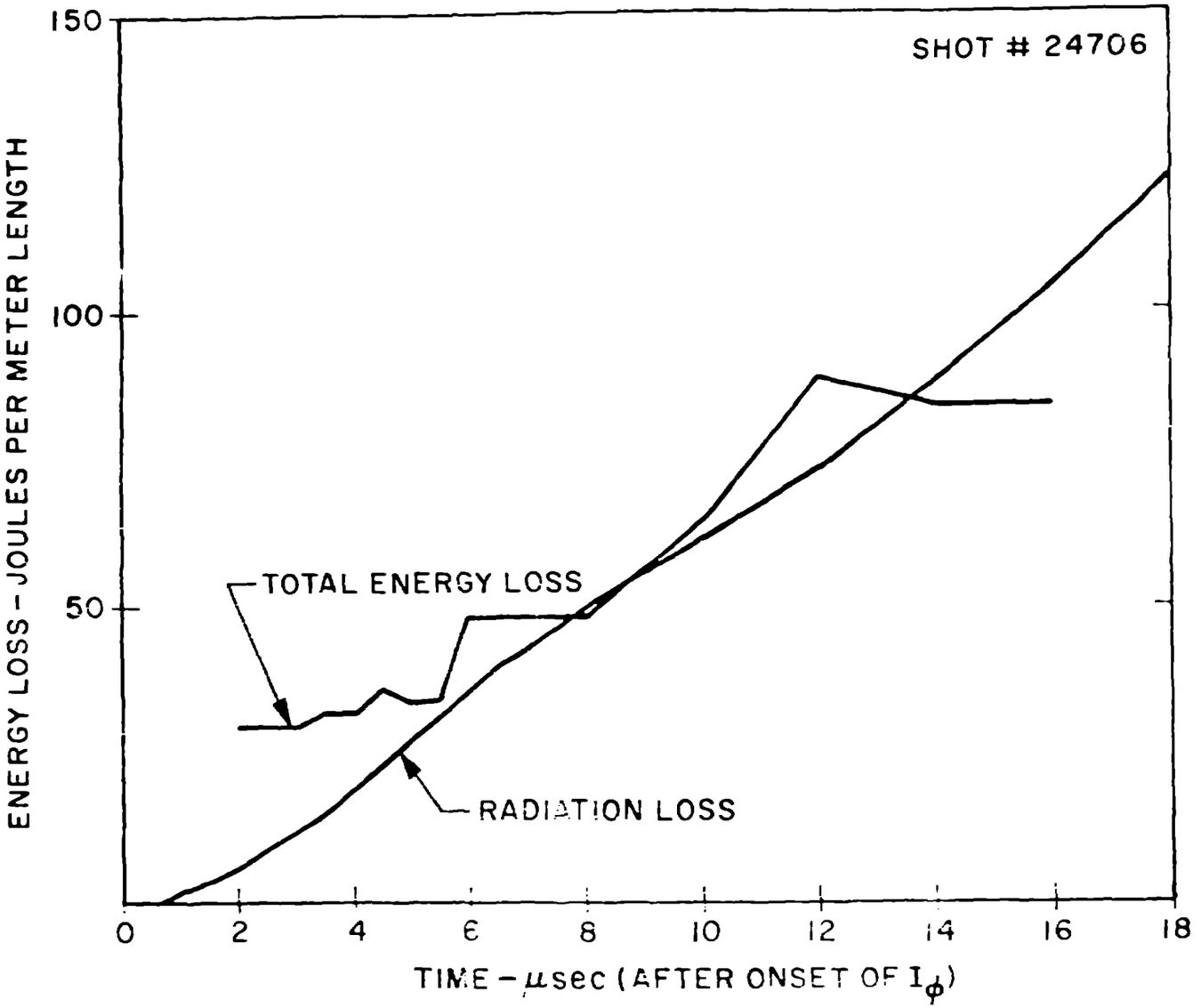
SHOT # 24706
150
100
50
ENERGY LOSS – JOULES PER METER LENGTH
TOTAL ENERGY LOSS
RADIATION LOSS
0
2
4
6
8
10
12
14
16
18
TIME – μsec (AFTER ONSET OF I_ϕ)

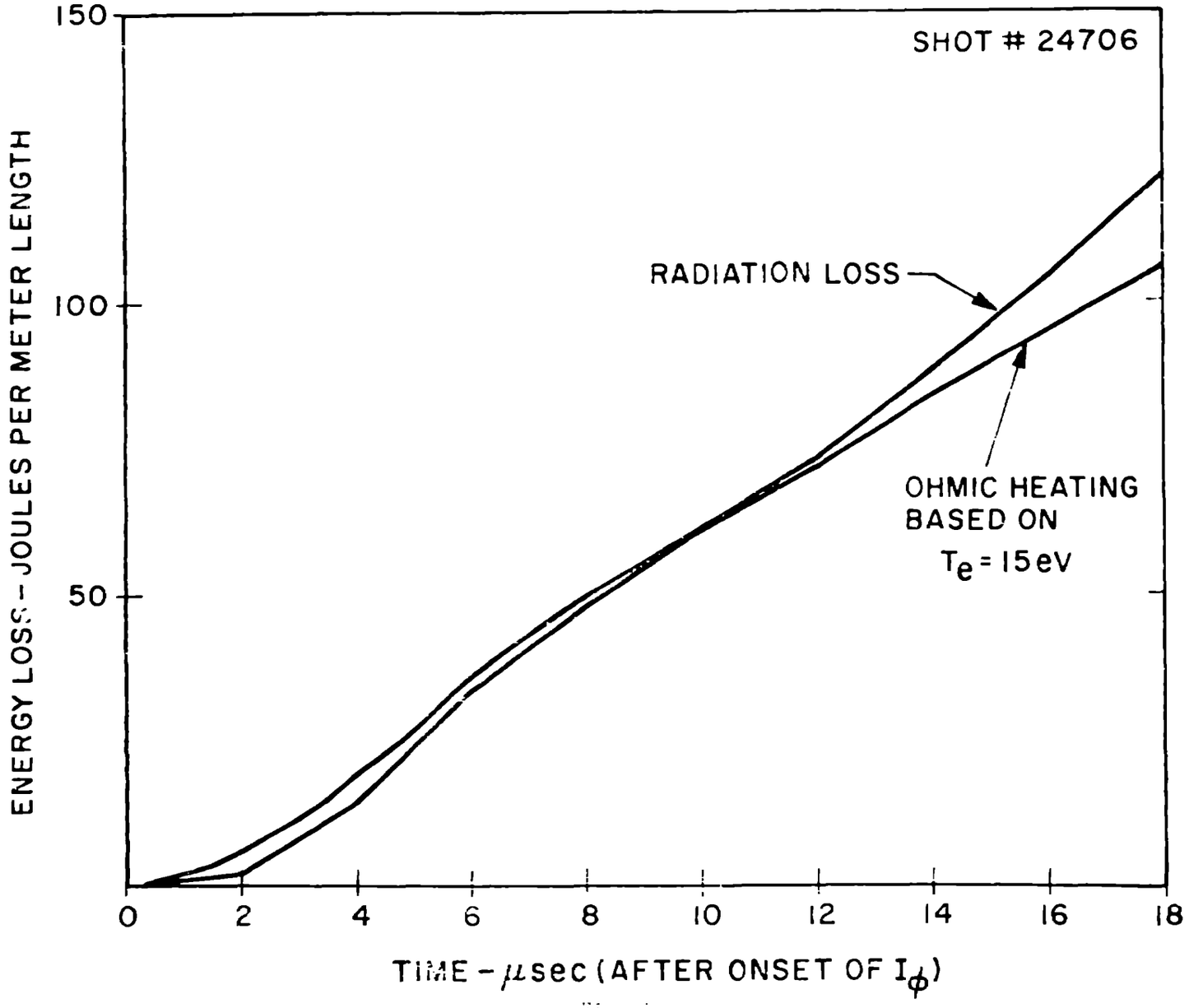

Fig. 4.

Curves comparing the measured radiation loss with the calculated ohmic input.

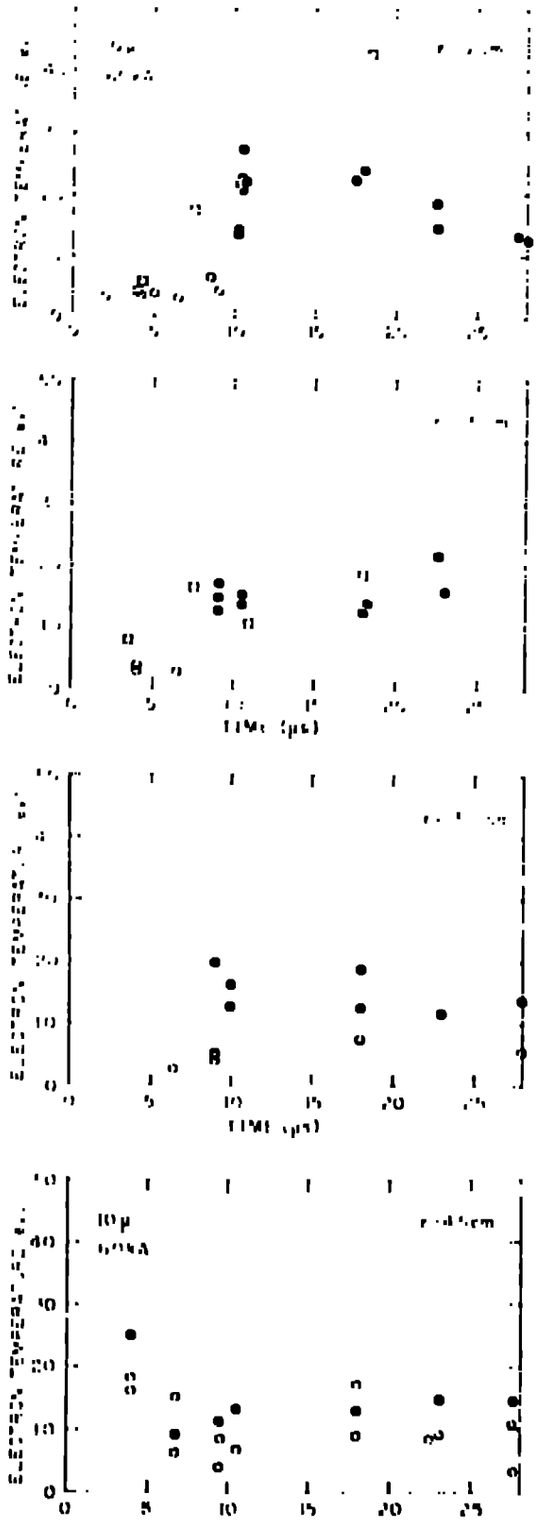

Fig. 5.
Thomson scattering measurement of electron temperature at (a) 0, (b) 1.5, (c) 3.0, and (d) 4.5 cm radius. Peak toroidal current 60 kA, filling pressure 10 mtorr of D_2.

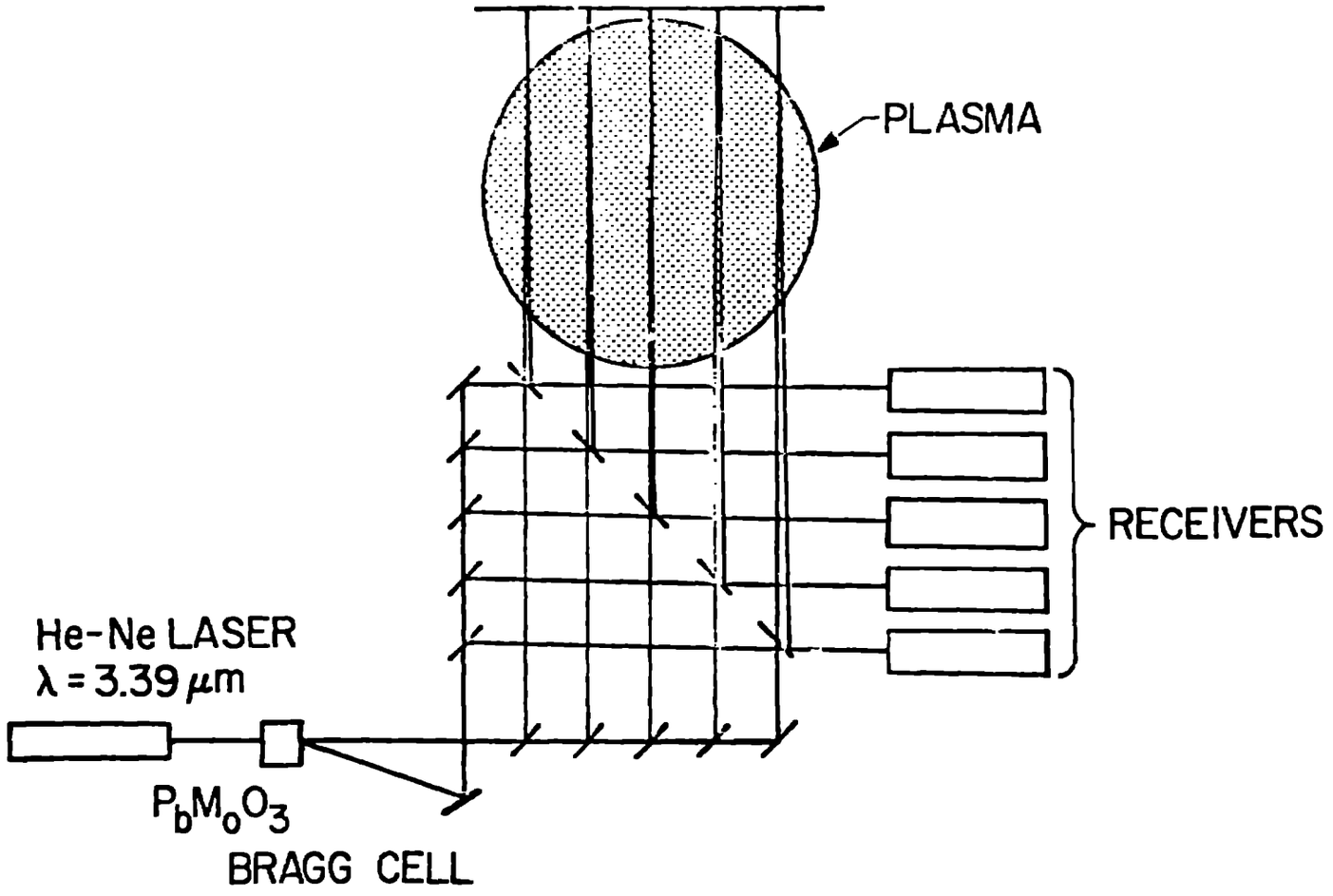

INTERFEROMETER SCHEMATIC

Fig. 6.
Schematic of the five channel interferometer.

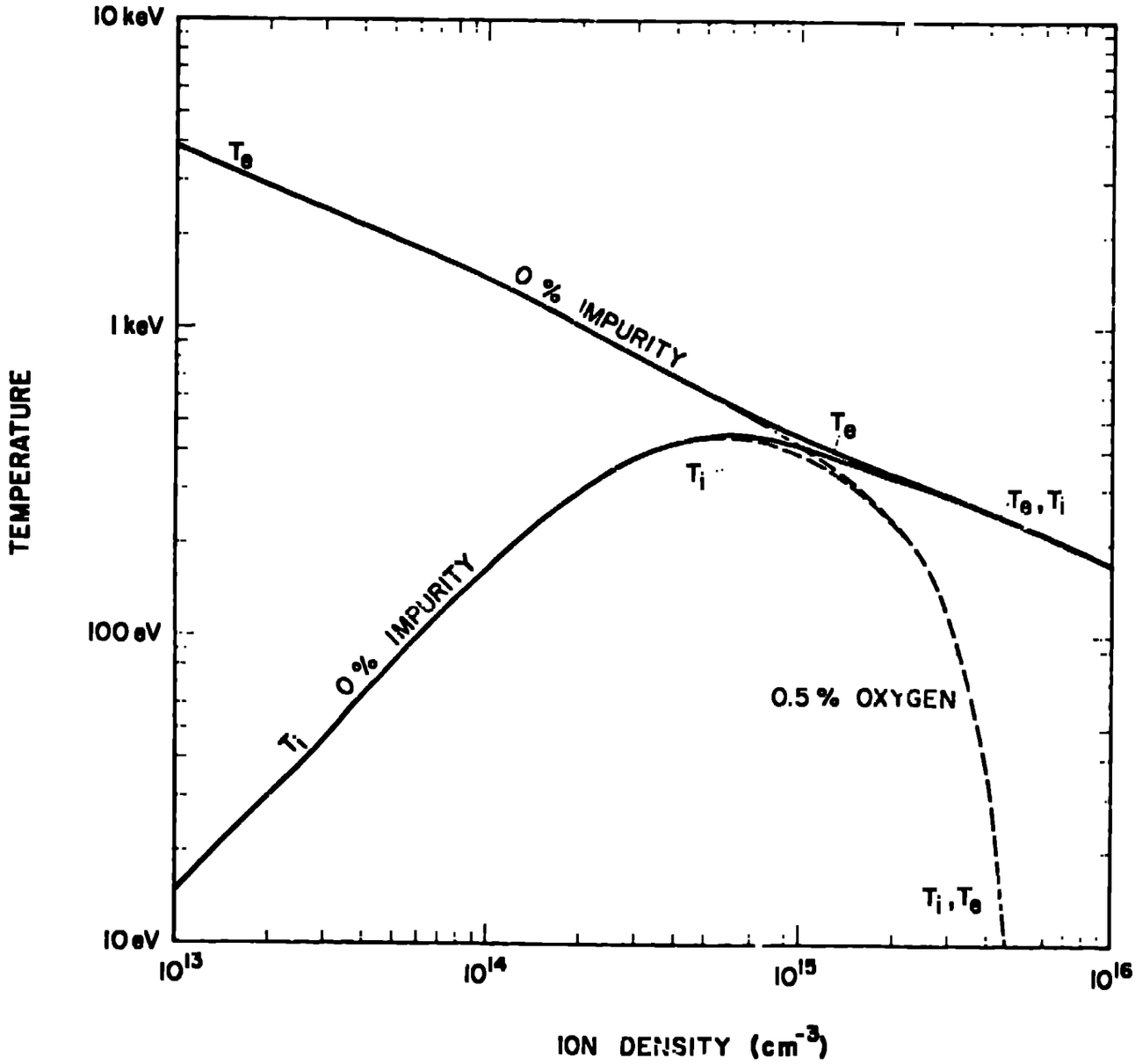

Fig. 7.
Ion and electron temperatures at 3 ms predicted by Imprad code for a uniform total current density of 3 kA/cm^2 which rises in 1 ms and decays with an e-folding time of 10 ms.

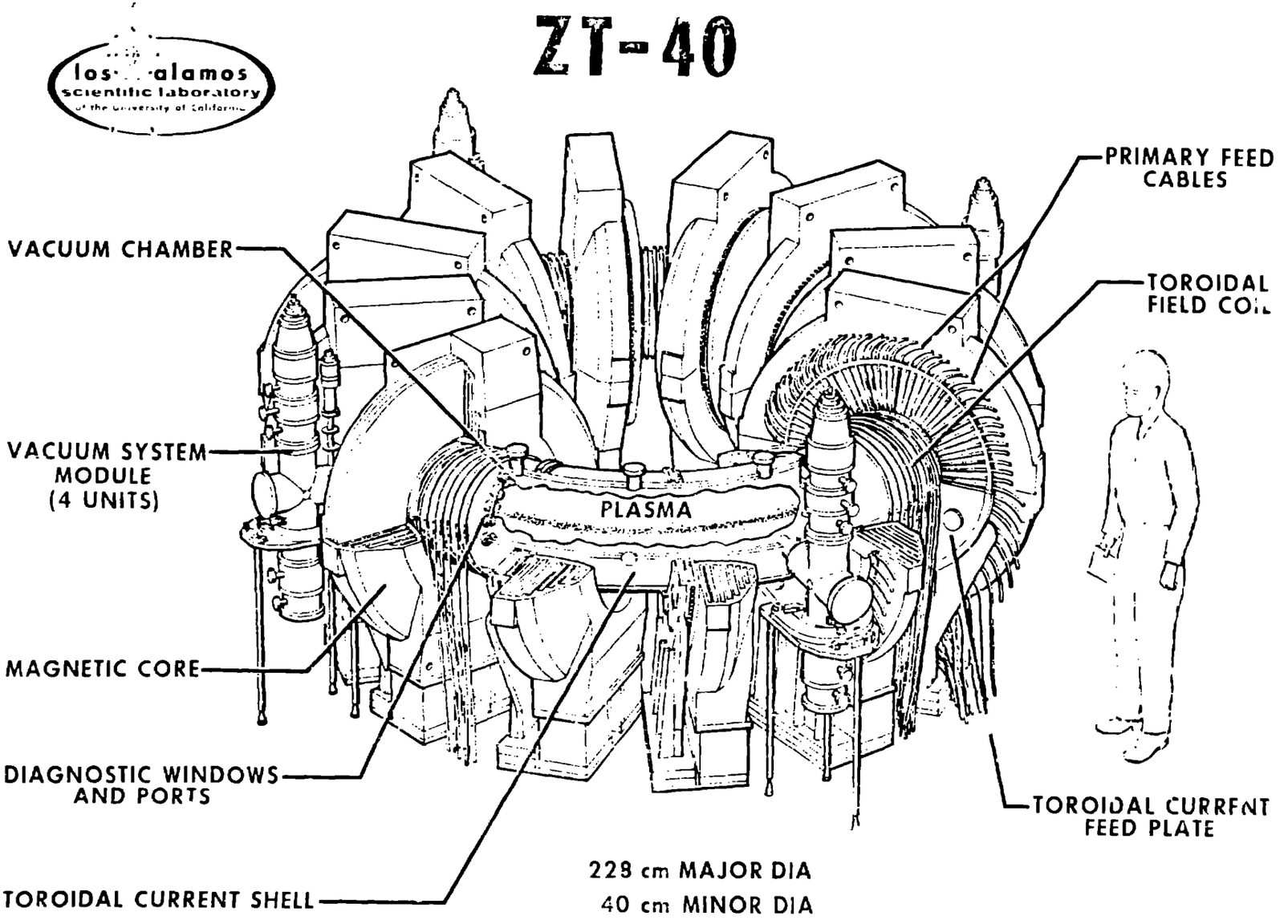

Fig. 3.
Artist's sketch of the front end of ZT-40.

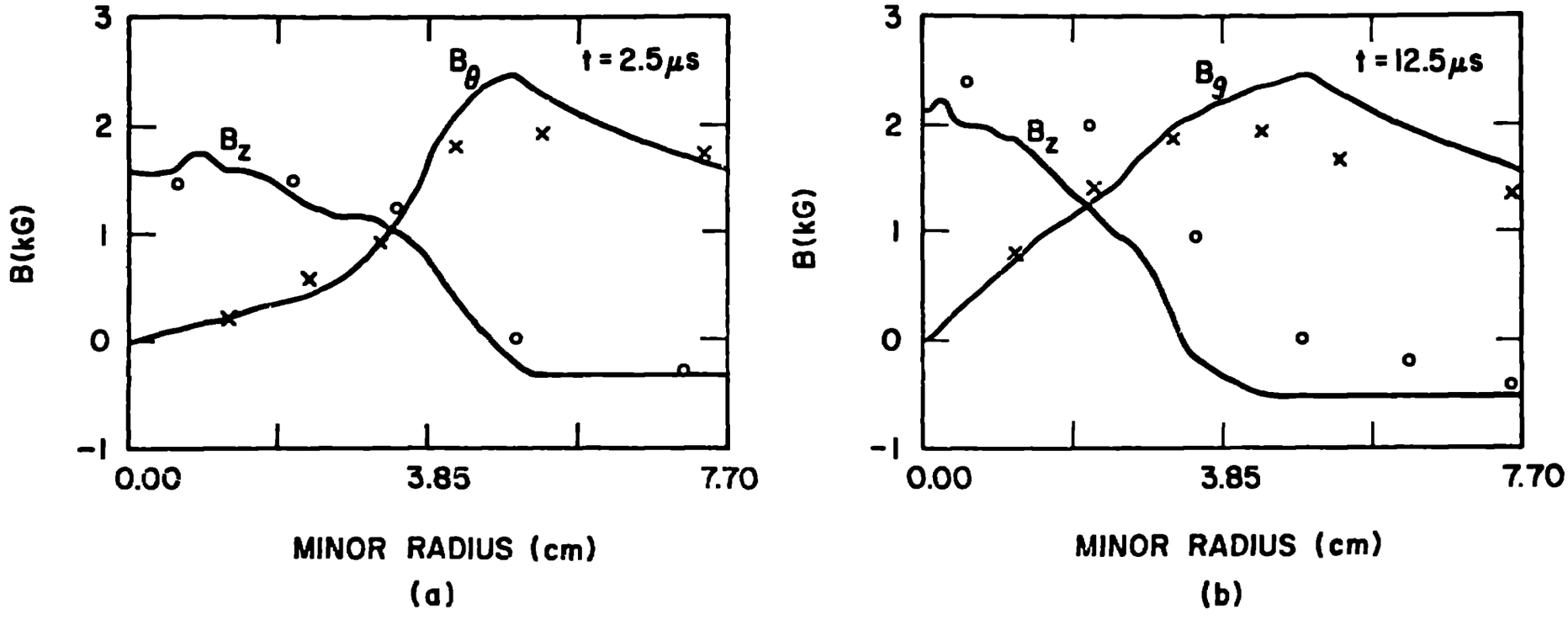

Fig. 9.
A comparison of the ZT-S fields theoretical calculations with the hybrid 1-D code. The x's are the experimental poloidal field data (to be compared with the B_θ of the cylindrical model) and the o's are the toroidal field data (compare with B_z). (a) Fields 2.5 μs after pinch current onset, (b) 12.5 μs after current onset.

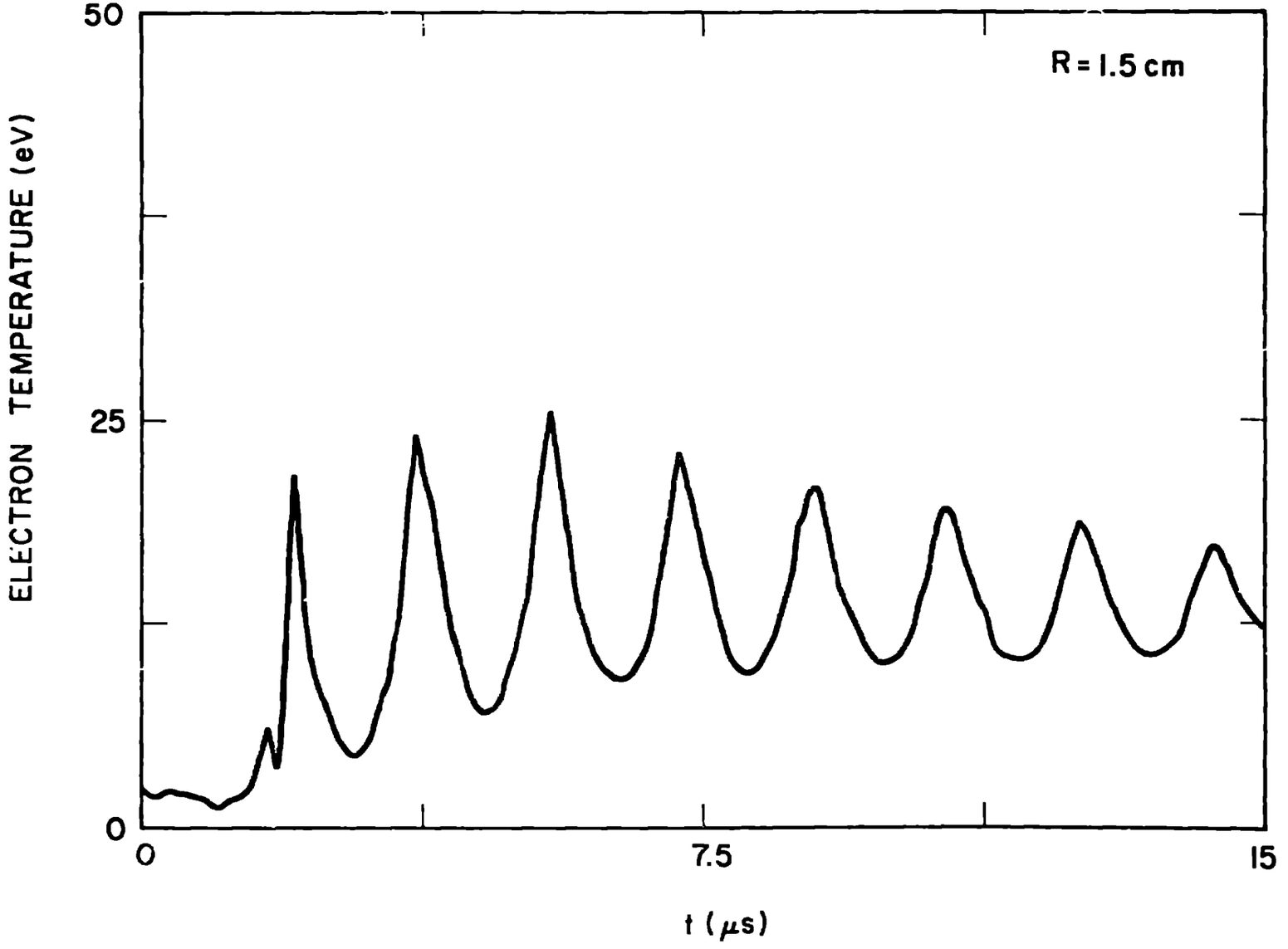

Fig. 10.
Electron temperature as calculated at r=1.5 cm in ZT-S.

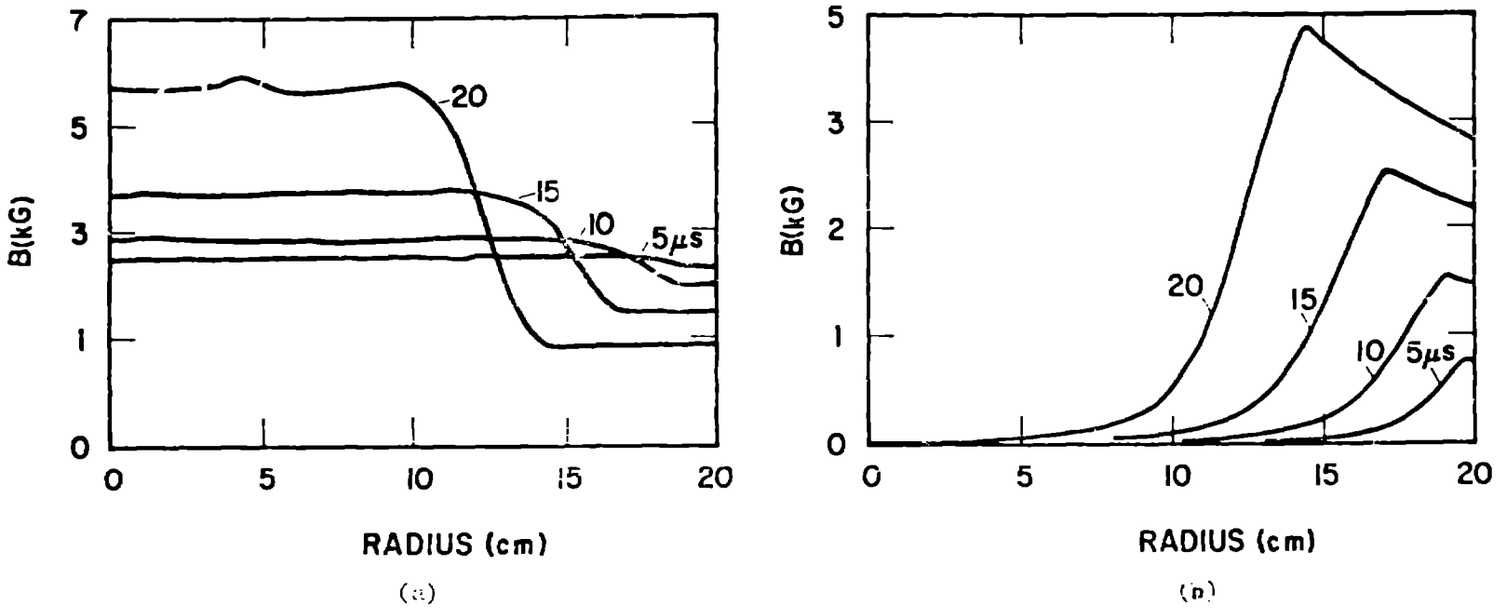

Fig. 11.
1-D hybrid code predictions of the field profile for ZT-40 with reversed-field programming. (a) axial field, (b) azimuthal field. Conditions: current risetime 20 μs, initial deuterium ion density 2.5×10^{15} cm^{-3}, initial bias field 3 kG, peak pinch current 600 kA.

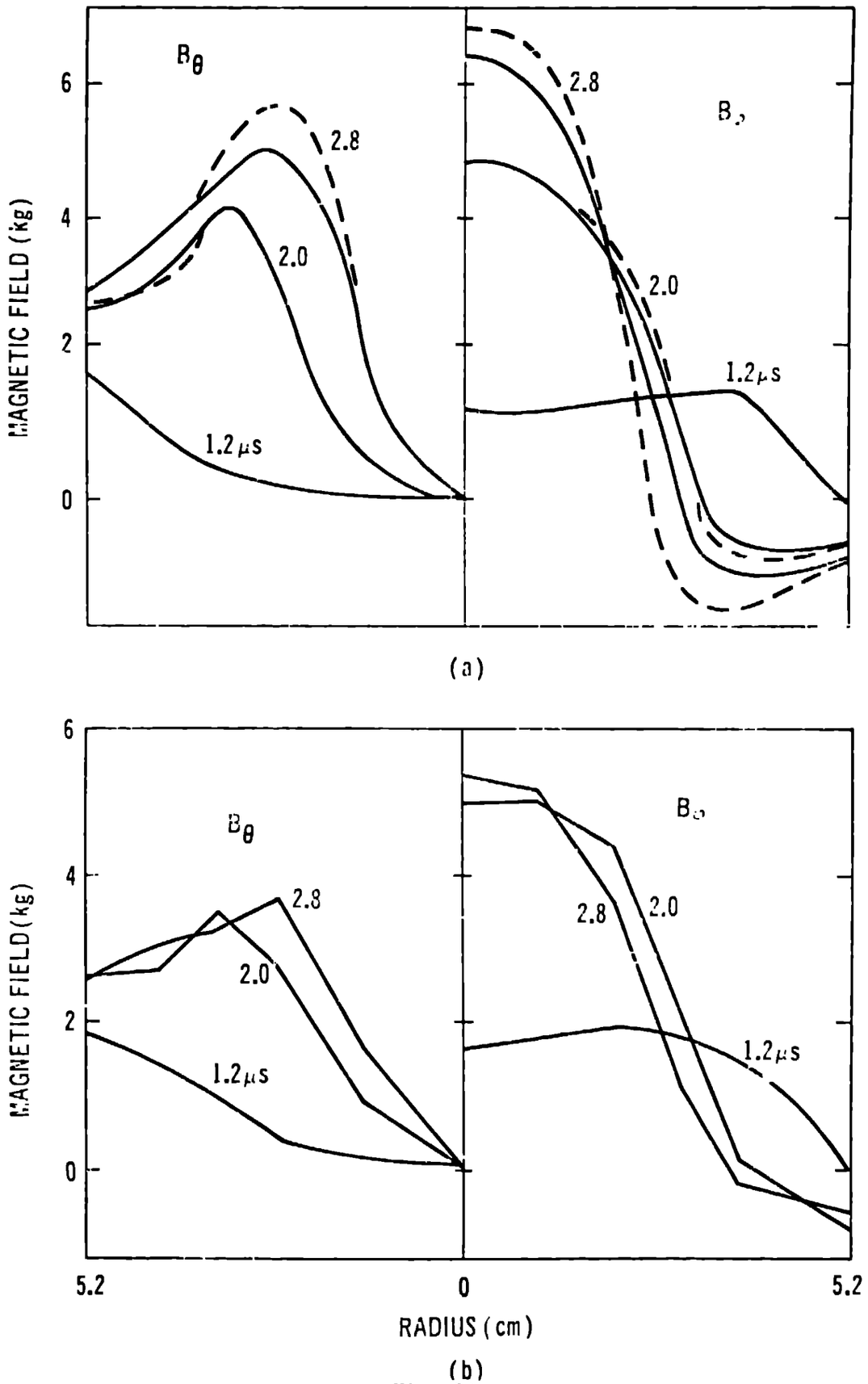

Fig. 12.
ZT-1 toroidal and poloidal field profiles: (a) 2-D toroidal calculation results with classical resistivity (---), and with the anomalous resistivity (——); (b) experimental curves (straight lines are drawn between data points).

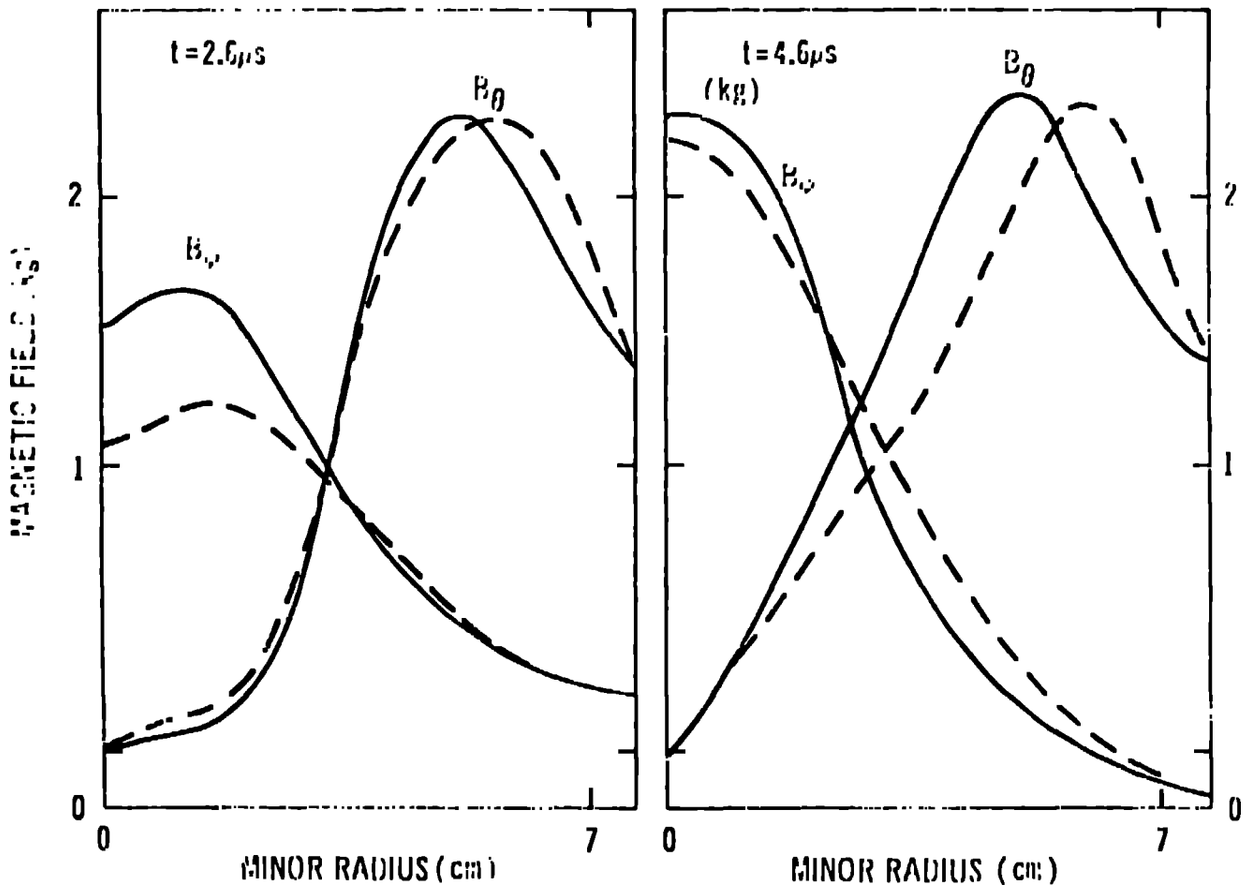

Fig. 13.

Toroidal and poloidal field profiles on the vertical radius (/2) of the poloidal plane are compared between the toroidal 2-D calculation (-) and experiment (---) at 2.6 and 4.6 μs for ST-5.

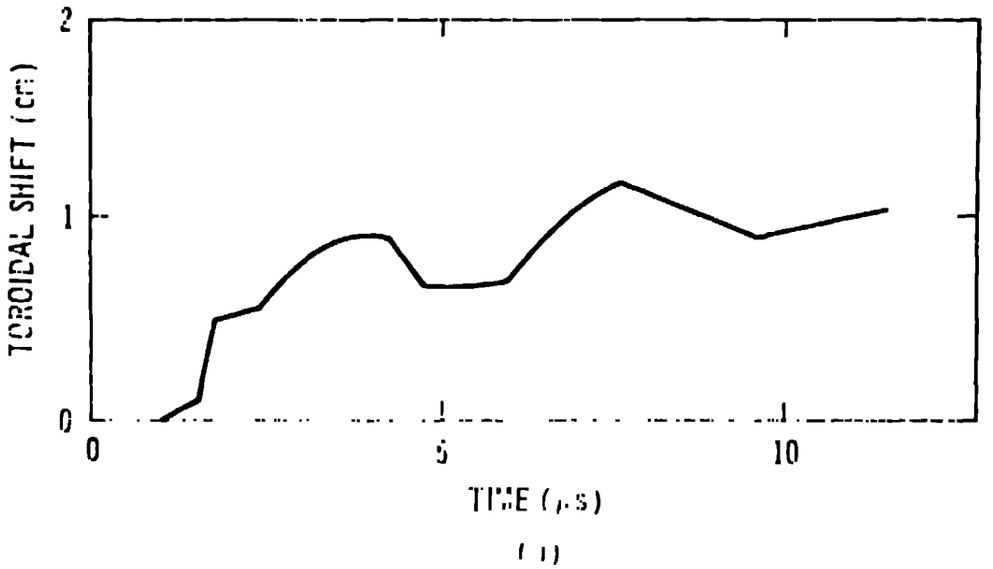

(a)

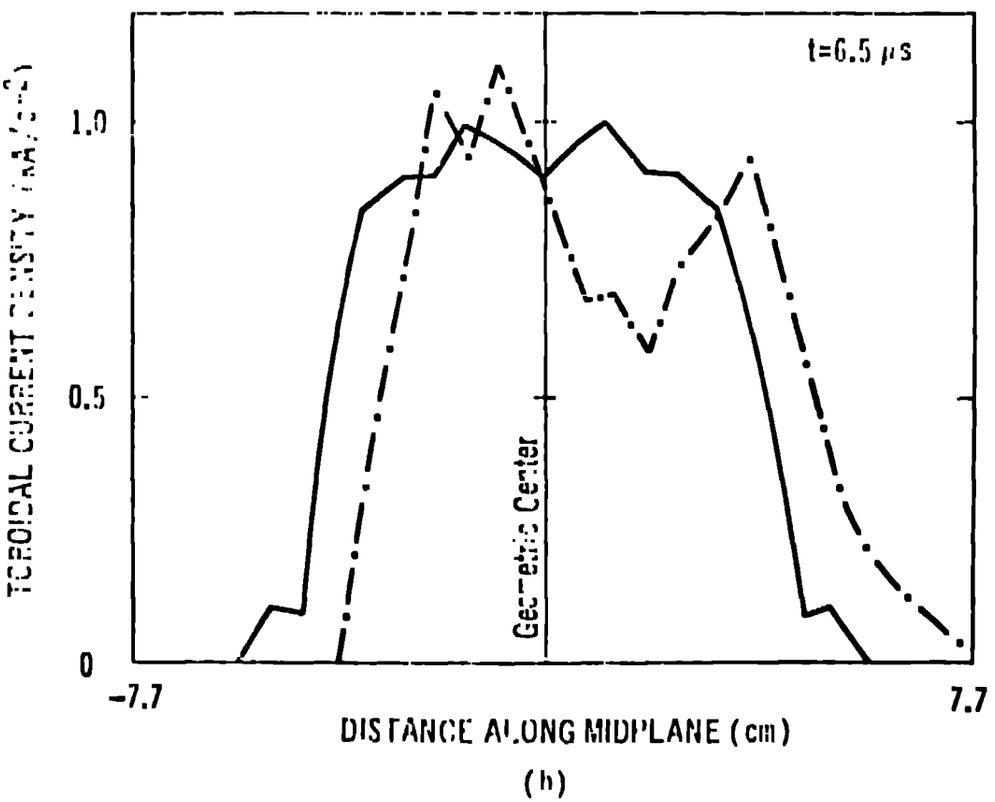

(b)

Fig. 14.
(a) Time trace of the toroidal shift of the magnetic axis. (ZT-S)
(b) Calculated toroidal current density profiles at 6.5 μs. The solid line represents the values on the vertical diameter ($\theta = \pm \pi/2$ of the poloidal plane, and the dashed line on the horizontal diameter. (ZT-S)

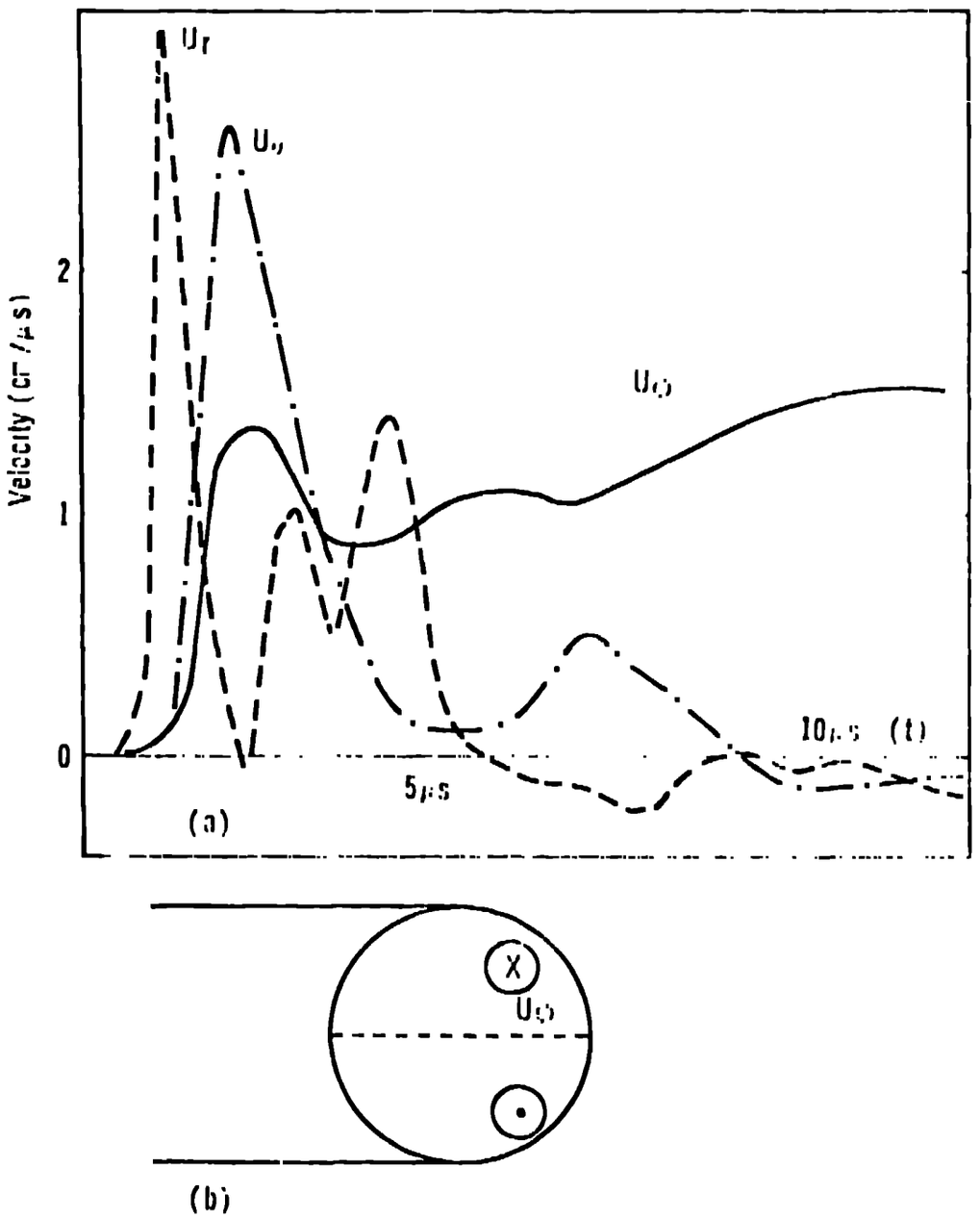

Fig. 16.
Time traces of the radial (U_r), axial/azimuthal (U_z) and toroidal velocities (U_φ at the point depicted in (b)). (CT-3)

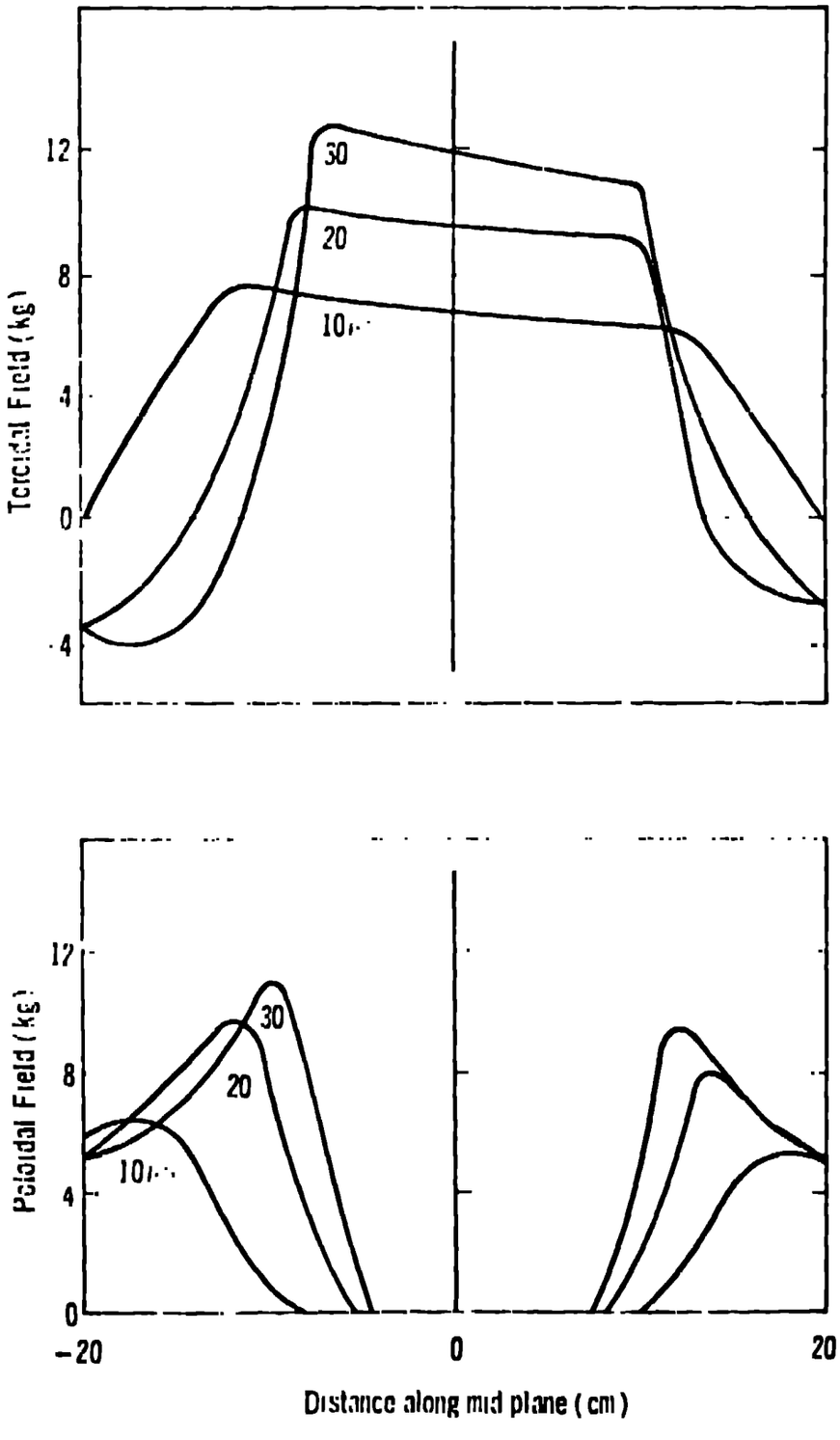

Fig. 16.
Predicted fields for 21-40 for reversed-field programming as calculated with the 2-D code. Current risetime 10 μs, initial deuterium ion density 1.50×10^{15} cm^{-3}, initial toroidal bias field 1 kG, peak current 500 kA.